Theoretical Studies of CO and NO Adsorption on Cu^+−ZSM-5 Zeolite

Holmann V. Brand, Antonio Redondo,* and P. Jeffrey Hay

Theoretical Division, MS B268, Los Alamos National Laboratory, Los Alamos, New Mexico 87545

Received: October 25, 1996; In Final Form: June 4, 1997[⊗]

Molecular models of the form $(H_2O)_n\cdots Cu^+\cdots X$, where $n = 1$, 2, 3 and X = CO, 2(CO), NO, $(NO)_2$, and H_2O are employed to investigate the catalytically active copper sites in Cu^+−ZSM-5 zeolite. Structures, binding energies and vibrational frequencies are calculated for these molecular models by density functional theory with gradient-corrected functionals. The calculated vibrational frequencies are compared to experimental infrared spectra of CO and NO adsorbed in Cu^+−ZSM-5 for each *n* value. The absence (presence) of an unpaired electron in the CO (NO) molecule is found to have effects in the structures, binding energies, and vibrational frequencies of the adsorbed species. Upon adsorption at a copper cation site, we find that, in agreement with experiment, (1) the stretching frequency of CO undergoes a small blue shift whereas that of NO is red shifted; (2) the formation of adsorbed dicarbonyl species is not as favored as the formation of adsorbed dinitrosyl species; and (3) the frequency separation between the antisymmetric and symmetric stretching modes is much smaller in the dicarbonyl species than in the dinitrosyl species. The choice of gradient-corrected functionals and the basis set used in this study is found to reproduce accurately the successive binding energies of $(H_2O)_n\cdots Cu^+$ when three or more ligands to the copper cation are present.

I. Introduction

Catalytic removal of nitrogen oxides (NO_x) from exhaust fumes has received a great deal of attention because of the detrimental effects of NO_x on the environment.[1] Copper-exchanged ZSM-5 zeolites have been reported[2] to have enhanced activity for the catalytic decomposition of NO_x in the presence of hydrocarbons and excess oxygen. Since then a great deal of interest has developed in these catalysts.

Copper cations are incorporated in the zeolite by either ion exchanging Na−zeolite samples with an aqueous solution of Cu^{2+} salts, such as copper acetate, or by exposing a dehydrated H−zeolite sample to CuCl. The first method results in activated Cu−zeolite samples containing both Cu^{2+} and Cu^+ cations whereas the second method produces Cu−zeolite samples containing only Cu^+ cations.[3] It should be pointed out that although both methods produce Cu−zeolite samples that are effective in catalytic removal of nitrogen oxides, the second method (i.e. the one producing Cu^+−zeolite samples) allows less ambiguity in mechanistic studies aimed at understanding the catalytic reactions that take place in NO_x removal.

The interaction of molecules at the copper sites has been probed by IR studies of carbon monoxide (CO) and nitric oxide (NO) adsorbed in Cu−ZSM-5 samples.[3−8] We focus our attention on IR studies of zeolite samples containing only Cu^+ cations.[3] IR spectra of NO adsorbed on Cu^+−ZSM-5 samples show a band at about 1810 cm^{-1} ascribed to the stretching mode of NO in the mononitrosyl complex $Cu^+(NO)$. By uptake of a second NO ligand, the dinitrosylic species $Cu^+(NO)_2$ is formed and gives rise to a pair of absorption bands at 1827 and 1734 cm^{-1} corresponding to the symmetric and antisymmetric stretching frequencies of the NO molecules in the dinitrosylic species. The IR spectra of CO adsorbed on Cu^+−ZSM-5 show a strong band at 2157 cm^{-1} which is ascribed to the stretching frequency of CO in the $Cu^+(CO)$ complex. Upon increase of CO pressure, the dicarbonylic species $Cu^+(CO)_2$ is formed having two bands at 2178 and 2151 cm^{-1} that are assigned to the symmetric and antisymmetric stretching frequencies of the adsorbed CO molecules.[3] It is interesting that the two bands assigned to the dinitrosylic species readily appear at room temperature whereas the two bands assigned to the dicarbonylic species appear only at relatively low temperature (70 K) and high CO pressure.[3]

In copper-exchanged ZSM-5 the location and coordination of the copper cations are not yet known. The most one can say from the experimental evidence is that the copper cations reside in locations accessible to molecules diffusing through the zeolite channels. Furthermore, experimental evidence suggests that the copper cations are mobile.[9,10] For this reason we have chosen not to employ the usual cluster models of the zeolite substrate[11,12] but rather molecular models which can simulate a number of configurations for the copper cations in the zeolite. Such models, as shown below, reproduce the well-established IR spectra of CO and NO adsorbed on Cu^+−ZSM-5.

Our molecular models employ water molecules to represent the oxygen atoms in the framework of the zeolite lattice interacting with the copper cation. In recent computational work,[13] Hass, Schneider, and co-workers employed computationally expensive zeolitic clusters and demonstrated that molecular models containing water molecules, such as the ones employed in our work, do indeed provide a very robust representation of the Cu^+ cation in the zeolite at a lower computational cost.

In this paper we wish to address the following questions by means of quantum mechanical calculations: (a) What are the factors that contribute to the relatively small blue shift observed in the stretching frequency of CO and the red shift in the stretching frequency of NO upon adsorption in Cu^+−ZSM-5? (b) Why is the adsorbed dinitrosyl species more readily formed than the dicarbonyl species in Cu^+−ZSM-5 at room temperature? (c) Why is the separation in frequency between the bands ascribed to antisymmetric and symmetric stretching modes of the dinitrosyl species larger than the corresponding separation in the modes of the dicarbonyl species? (d) What are the relative

[⊗] Abstract published in *Advance ACS Abstracts,* September 1, 1997.

S1089-5647(96)03327-5 CCC: $14.00

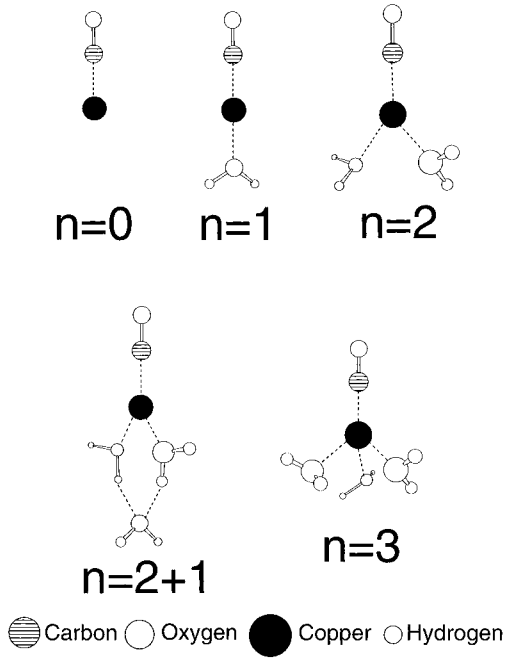

Figure 1. $(H_2O)_n\cdots Cu^+\cdots CO$ molecular models.

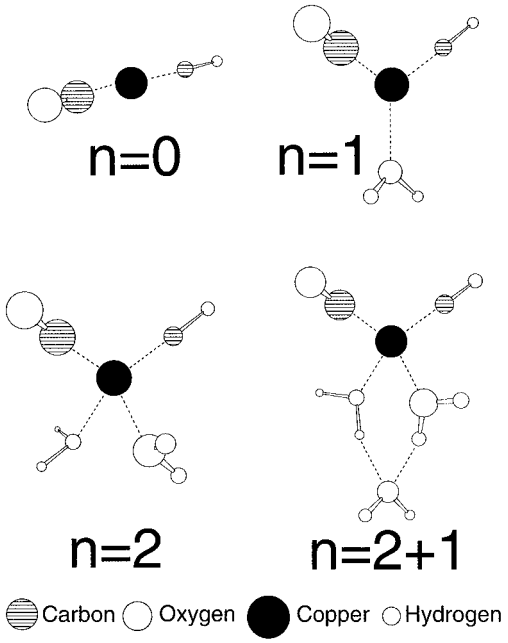

Figure 2. $(H_2O)_n\cdots Cu^+\cdots 2(CO)$ molecular models.

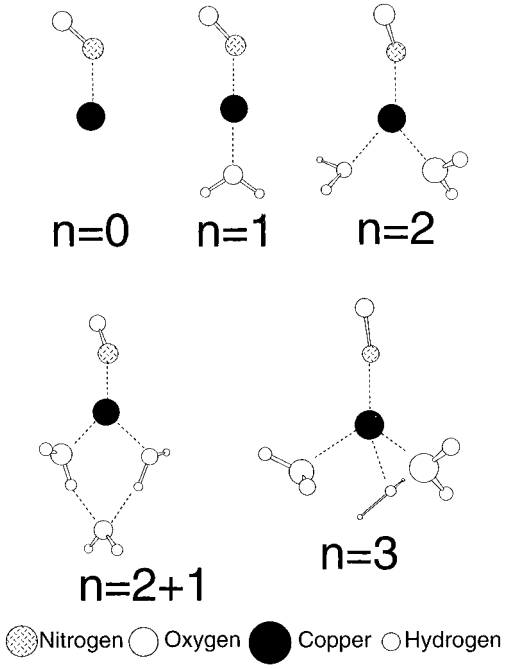

Figure 3. $(H_2O)_n\cdots Cu^+\cdots NO$ molecular models.

binding energies of NO and CO to the Cu^+ cation and what accuracy can be expected from the computational method employed?

This paper is organized as follows: section II describes the computational method and molecular clusters employed; section III contains the results of the computations and comparison with experiment; section IV presents a discussion of the relevance of the results; and finally, conclusions are summarized in Section V.

II. Computational Method

As mentioned above, our goal is to reproduce the IR spectra of CO and NO adsorbed on copper-exchanged Cu^+-ZSM-5 zeolite without making any assumptions about cation location. To model the transfer of negative charge from the zeolite framework to the copper cation, we place water molecules about the copper cation thus allowing the lone pairs on the oxygen atoms of the water molecules to donate negative charge to the copper cation (see Figures 1−4). The stretching vibrational frequency of the CO and NO molecules interacting with Cu^+ is then calculated as a function of the number of water molecules coordinated to the cation. Thus the number of water molecules coordinated to the Cu^+ cation is varied, and the calculated frequency shifts of CO and NO interacting with Cu^+ are compared with the experimental values of the measured spectra.

To correct for the inherent errors in the calculated frequencies, as compared to experiment, we applied empirical scaling factors to the calculated harmonic stretching vibrational frequencies of the adsorbed molecules CO and NO in the $(H_2O)_n\cdots Cu^+\cdots X$ models. The scaling factor for the calculated CO frequencies in the $(H_2O)_n\cdots Cu^+\cdots X$ models was obtained by comparing the calculated stretching frequencies of the free CO and CO^+ molecules with their corresponding experimentally observed gas phase values of 2143[3] and 2214 cm^{-1}.[14] Similarly, the scaling factor for the calculated NO frequencies in the $(H_2O)_n\cdots Cu^+\cdots X$ models was obtained by comparing the calculated stretching frequencies of the free NO and NO^+ molecules with their corresponding experimentally observed gas phase values of 1876[3] and 2354 cm^{-1}.[15] This scaling procedure is based on the observed trend that the error in the calculated vibrational frequencies of similar internal coordinates is systematic within any particular computational method[16] and can therefore be corrected by a transferable scaling factor determined empirically.

To describe the interaction between the copper cation and the adsorbed molecules, we employ gradient-corrected density functional techniques which have proved to be a relatively inexpensive means of including electron correlation.[16,17] In particular, the B-LYP approximation, which treats the exchange energy using the gradient-corrected functional of Becke[18] and the correlation energy with the gradient-corrected functional of Lee, Yang, and Parr[19] was found to produce harmonic frequencies that were in good agreement[16,17] with observed fundamentals when the 6-31G* basis set[20] was employed.

In the work reported herein we applied the B-LYP method with the 6-31G* basis set to the molecular models and calculated the optimized geometric parameters by minimizing the total energy of the system. Then, at the optimum geometries, we

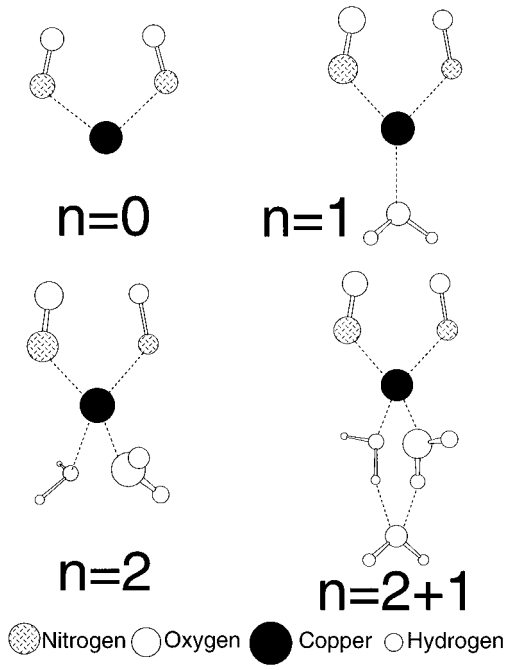

Figure 4. $(H_2O)_n\cdots Cu^+\cdots(NO)_2$ molecular models (singlet state shown).

calculated the corresponding harmonic frequencies. All the optimized geometries of the molecular models containing the adsorbed species CO, 2(CO), NO, and $(NO)_2$ were verified to be true local minima by the absence of imaginary frequencies. The basis for Cu was taken from the Gaussian basis of Wachters[21] for the $3d^{10}$ $4s^1$ state of Cu. Two additional primitive functions were added to describe the 4p orbital with the same exponents ($\zeta = 0.1133$ and 0.0407) as the most diffuse s functions in the original basis. Finally an additional diffuse 3d function ($\zeta = 0.1491$) introduced by Hay[22] was employed. The (14s 11p 6d) primitive basis was contracted to (6s 7p 3d) using a general contraction for the innermost primitives and allowing the outermost 3s, 5p, and 2d primitive functions to remain uncontracted. All the calculations were performed with the Gaussian 94 package[23] employing default grids. Tests with finer grids resulted in essentially identical binding energies and vibrational frequencies at a much higher computational cost.

The molecular models considered in this work are denoted $(H_2O)_n\cdots Cu^+\cdots X$ where n is the number of water molecules and X = CO, 2(CO), NO, $(NO)_2$, or H_2O. Thus the label $(H_2O)_n\cdots Cu^+\cdots CO$ refers to complexes containing one adsorbed CO molecule on the Cu^+ cation. These $(H_2O)_n\cdots Cu^+\cdots CO$ complexes are displayed in Figure 1 in their optimized geometry parameters. Similarly the label $(H_2O)_n\cdots Cu^+\cdots 2(CO)$ denotes the models containing two adsorbed CO molecules (see Figure 2). Likewise the $(H_2O)_n\cdots Cu^+\cdots NO$ and $(H_2O)_n\cdots Cu^+\cdots(NO)_2$ complexes, displayed in Figures 3 and 4, contain one and two adsorbed NO molecules on the Cu^+ cation, respectively. It should be pointed out that all the water molecules in the cases $n = 1$, $n = 2$, and $n = 3$ are ligands to the Cu^+ cation whereas in the $n = 2 + 1$ conformation only the first two water molecules are ligands to the Cu^+ cation while the third one is hydrogen bonded to the first two waters. Consequently, the $n = 2 + 1$ case allows more charge transfer to the Cu^+ cation than the $n = 2$ case while maintaining the number of ligands to the Cu^+ cation equal to that of the $n = 2$ arrangement. The $(H_2O)_{2+1}\cdots Cu^+\cdots X$ models are less floppy than the $n = 2$ and $n = 3$ models and therefore less problematic during geometry optimization.

The binding energy of CO to the Cu^+ cation in the $(H_2O)_n\cdots Cu^+\cdots CO$ models is defined by

$$\Delta E^e = E[(H_2O)_n\cdots Cu^+] + E[CO] - E[(H_2O)_n\cdots Cu^+\cdots CO]$$

where $[E[\ ]$ means the energy of the complex or molecule at its optimized geometry calculated with the B-LYP approximation. The zero-point energy contribution to the binding energy is calculated according to

$$\Delta ZPE = ZPE[(H_2O)_n\cdots Cu^+] + ZPE[CO] - ZPE[(H_2O)_n\cdots Cu^+\cdots CO]$$

where ZPE[ ] is the zero-point energy of the complex or molecule calculated at its optimized geometry.

When two CO molecules adsorb on the Cu^+ cation, the energy needed to remove one CO molecule is defined by

$$\Delta E^e = E[(H_2O)_n\cdots Cu^+\cdots CO] + E[CO] - E[(H_2O)_n\cdots Cu^+\cdots 2(CO)]$$

The zero-point energy contribution to this energy is

$$\Delta ZPE = ZPE[(H_2O)_n\cdots Cu^+\cdots CO] + ZPE[CO] - ZPE[(H_2O)_n\cdots Cu^+\cdots 2(CO)]$$

Similarly, the energy needed to remove both CO molecules is obtained by

$$\Delta E^e = E[(H_2O)_n\cdots Cu^+] + 2E[CO] - E[(H_2O)_n\cdots Cu^+\cdots 2(CO)]$$

with its zero-point energy correction defined by

$$\Delta ZPE = ZPE[(H_2O)_n\cdots Cu^+] + 2ZPE[CO] - ZPE[(H_2O)_n\cdots Cu^+\cdots 2(CO)]$$

Replacing C by N in the above equations results in expressions defining the binding energies in the case of adsorption of one or two NO molecules on the Cu^+ cation in the $(H_2O)_n\cdots Cu^+$ models.

The relative stability of CO adsorption on Cu^+ through the C atom versus the O atom was investigated by comparing the energies of the $(H_2O)_n\cdots Cu^+\cdots CO$ and $(H_2O)_n\cdots Cu^+\cdots OC$ molecular models at their corresponding optimized geometries for $n = 0$, 1, and 2. Similarly, the relative stability of NO adsorption on Cu^+ through the N atom versus the O atom was examined by comparing the energies of the $(H_2O)_n\cdots Cu^+\cdots NO$ and $(H_2O)_n\cdots Cu^+\cdots ON$ molecular models at their corresponding optimized geometries for $n = 0$, 1, and 2. In addition, when two NO molecules are adsorbed, the energy of the triplet electronic state of the $(H_2O)_n\cdots Cu^+\cdots(NO)_2$ molecular models was calculated for $n = 0$, 1, and 2 at optimized geometries and was compared with the corresponding singlet state energy for each n. The $(H_2O)_n\cdots Cu^+\cdots(NO)_2$ models in the singlet and triplet state will be referred to as singlet X = $(NO)_2$ and triplet X = $(NO)_2$, respectively.

III. Results

Figures 1−5 show the molecular models $(H_2O)_n\cdots Cu^+\cdots X$ with X = CO, 2(CO), NO, $(NO)_2$, and H_2O. Their geometrical parameters are listed in Table 1. Upon adsorption at the Cu^+ cation in the $(H_2O)_n\cdots Cu^+$ models, the CO molecule forms a linear $Cu^+\cdots CO$ bond for all n whereas the NO molecule forms a bent $Cu^+\cdots NO$ bond. The linearity of the $Cu^+\cdots CO$ bond

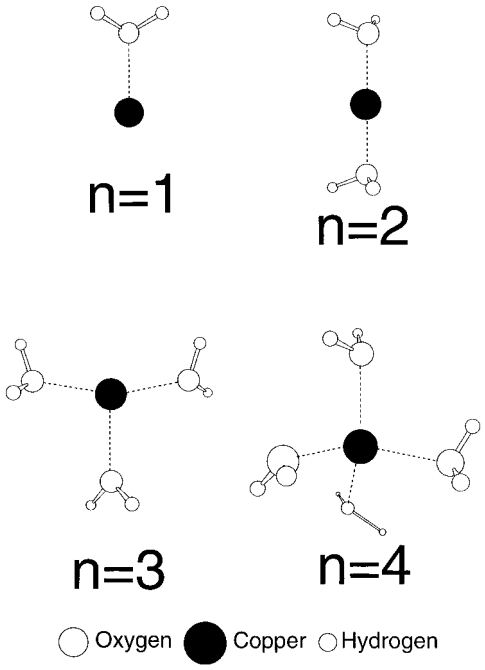

Figure 5. $(H_2O)_n\cdots Cu^+$ complexes.

persists even when two CO molecules are adsorbed (Figure 2). As listed in Table 1, the $Cu^+\cdots CO$ bond deviates from linearity by less than 4° when X = 2(CO). Because the $Cu^+\cdots CO$ bond is linear in the $(H_2O)_n\cdots Cu^+\cdots CO$ molecular models, the optimized geometrical parameters of the $n = 1$, 2, $2 + 1$, and 3 cases were found to have C_s, C_2, C_2, and C_3 symmetry, respectively, even though no symmetry constraints were imposed during the optimization. For X = 2(CO) the $n = 1$, 2, and $2 + 1$ cases were also found to have C_s, C_2, and C_2 symmetry, respectively.

Comparing the adsorbed CO and NO molecules, Table 1 reveals that when $n = 0$ the r(CO) and r(NO) bond lengths of the adsorbed CO and NO molecules in the X = CO, 2(CO), NO, and $(NO)_2$ models are shorter than those calculated for the free CO and NO molecules. Since the calculated bond lengths of free CO^+ and NO^+ are shorter than those of free CO and NO, it would appear that the adsorbed CO and NO molecules donate electron charge to the Cu^+ cation. Also evident in Table 1 is the trend that the bond lengths of the adsorbed CO and NO molecules increase as the number of water molecules increases. Hence, it appears that electron charge transfer from the adsorbed CO and NO to the Cu^+ cation is less favored as n increases. Because changes in bond length are more noticeable in the case of adsorbed NO than in the case of adsorbed CO, it can be expected that charge transfer is enhanced when the adsorbed molecule is NO.

The distance between the Cu^+ cation and the water molecules coordinated to it, denoted $r(Cu^+\cdots O_w)$ in Table 1, increases as n is increased in the sequence $n = 1$, 2, 3. This increase in $r(Cu^+\cdots O_w)$ suggests that there may be repulsion among the water molecules coordinated to the Cu^+ cation. As n is increased in the sequence 1, 2, and 3, the $r(Cu^+\cdots C)$ and $r(Cu^+\cdots N)$ bond lengths increase for X = 2(CO) and triplet X = $(NO)_2$ and decrease for X = CO, X = NO, and singlet X = $(NO)_2$. Hence, for X = 2(CO) and triplet X = $(NO)_2$ a repulsion similar to that among the water molecules seems to be occurring between the two adsorbed CO molecules and between the two adsorbed NO molecules. By contrast, the fact that the pattern of variation in $r(Cu^+\cdots N)$ bond length for singlet X = $(NO)_2$ is that of a single adsorbed molecule, such as X = CO or X = NO, is consistent with the trend that the $r(O\cdots O)$ distance between the two adsorbed NO molecules in the singlet state resembles the calculated $r(O\cdots O)$ distance in the free NO dimer even when $n = 0$.

According to Table 1, the $C\cdots Cu^+\cdots C$ angle decreases sharply from 180 to 129° as one water molecule is added, but further addition of water molecules to form the $n = 2$ and $n = 2 + 1$ models results in a $C\cdots Cu^+\cdots C$ angle that is virtually constant at about 122° and is in good agreement with the experimental estimate of 120°.[3] For $n = 0$, the two adsorbed NO molecules in the triplet state lie on opposite sides of the Cu^+ cation forming a $N\cdots Cu^+\cdots N$ angle equal to 180°, as in the case of two adsorbed CO molecules, while in the singlet state the $N\cdots Cu^+\cdots N$ angle is only 97.2°. However, as water molecules are added, the $N\cdots Cu^+\cdots N$ angle of the triplet state approaches the value of the singlet state so that at $n = 2 + 1$ they only differ by 6.1°. The calculated values for the $N\cdots Cu^+\cdots N$ angle of the singlet and triplet states when water molecules are present are in reasonable agreement with the experimentally derived value of 104°.[3] We point out that for X = $(NO)_2$ the triplet electronic state is less stable than the singlet state by 3.1, 5.1, and 5.7 kcal/mol for $n = 1$, 2, and $2 + 1$, respectively. Only for the case $n = 0$ is the triplet state more stable (7.6 kcal/mol) than the singlet state because it allows the two adsorbed NO molecules to be on opposite sides of the Cu^+ cation thereby minimizing repulsion.

The optimized geometrical parameters of $(H_2O)_n\cdots Cu^+\cdots X$ with X = OC or X = ON, that is, adsorbtion through the O atom, are not reported in Table 1 because such configurations were not energetically favorable. Specifically, CO adsorption on Cu^+ through the O atom was less stable than through the C atom by 22−26 kcal/mol for $n = 0$, 1, and 2. Similarly, NO adsorption on Cu^+ through the O atom was less stable than through the N atom by about 14 kcal/mol for $n = 0$ and 1. The optimized geometrical parameters of $(H_2O)_n\cdots Cu^+\cdots X$ with X = OC or X = ON were verified to be local minima by the absence of imaginary frequencies in their normal modes.

The Mulliken charges of selected atoms in the $(H_2O)_n\cdots Cu^+\cdots X$ models are listed in Table 2. The charge of the Cu^+ cation is denoted by $q(Cu^+)$. The charge of each adsorbed CO and NO molecule is denoted by $q(C) + q(O)$ and $q(N) + q(O)$ where $q(C)$, $q(O)$, and $q(N)$ are the Mulliken charges of the individual C, O, and N atoms in the adsorbed CO and NO molecules. As the number of water molecules n is increased, the charges of the Cu^+ cation and the adsorbed CO and NO molecules decrease, thereby suggesting that electron charge is transferred from the water molecules to the Cu^+ cation and the adsorbed CO and NO molecules. This charge transfer is particularly noticeable in the case of NO adsorption. These changes in Mulliken charges are consistent with the changes in bond lengths mentioned above regarding the data of Table 1.

The frequencies of the $(H_2O)_n\cdots Cu^+\cdots X$ models with X = CO and X = 2(CO) are listed in Table 3. For CO frequencies we calculated a scaling factor of $\sigma = 1.0206$. As reported in Table 3, the CO molecule undergoes a 90 cm^{-1} increase in its stretching frequency ω(CO) upon interaction with the Cu^+ cation in the $n = 0$ model. Since the stretching frequency of CO^+ is higher than that of CO, the blue frequency shift of CO in $Cu^+\cdots$-CO suggests an electronic charge transfer from the adsorbed CO to the Cu^+ cation. This increase in ω(CO) in $Cu^+\cdots CO$ correlates with the decrease in its r(CO) bond length (see Table 1) mentioned above. Similarly, the decrease in ω(CO) in $(H_2O)_n\cdots Cu^+\cdots CO$ as n is increased correlates with a concurrent lengthening in the r(CO) bond length. As n is increased, the scaled ω(CO) values approach the experimental 2157 cm^{-1} band

TABLE 1: Partial List of Geometrical Parameters of Fully Optimized $(H_2O)_n\cdots Cu^+\cdots X$ Models[a]

parameter	$n = 0$	$n = 1$	$n = 2$	$n = 2 + 1$	$n = 3$
			X = CO[b]		
r(CO)	1.140	1.143	1.148	1.150	1.152
r($Cu^+\cdots$C)	1.875	1.843	1.835	1.829	1.828
r($Cu^+\cdots O_w$)		1.926	2.061	2.033	2.145
a($Cu^+\cdots$CO)	180.0	179.7	180.0	180.0	180.0
			X = $(CO)_2$		
r(CO)	1.140	1.144	1.147	1.148	
r($Cu^+\cdots$C)	1.909	1.917	1.922	1.923	
r(C···C)	3.817	3.456	3.365	3.356	
r(O···O)	6.096	5.462	5.297	5.303	
r($Cu^+\cdots O_w$)		2.032	2.149	2.139	
a($Cu^+\cdots$CO)	180.0	176.9	176.2	177.0	
a(C···$Cu^+\cdots$C)	180.0	128.6	122.1	121.5	
			X = NO[c]		
r(NO)	1.159	1.171	1.180	1.182	1.184
r($Cu^+\cdots$N)	1.911	1.841	1.833	1.828	1.841
r($Cu^+\cdots O_w$)		1.925	2.057, 2.038	2.025	2.089, 2.098, 2.259
a($Cu^+\cdots$NO)	130.5	137.1	139.8	140.8	139.2
			X = $(NO)_2$[d]		
r(NO)	1.163(s), 1.162(t)	1.170(s), 1.171(t)	1.176(s), 1.178(t)	1.177(s), 1.179(t)	
r($Cu^+\cdots$N)	2.003(s), 1.786(t)	1.974(s), 1.855(t)	1.955(s), 1.910(t)	1.951(s), 1.909(t)	
r(N···N)	3.004(s), 3.571(t)	2.823(s), 3.283(t)	2.783(s), 2.905(t)	2.774(s), 2.854(t)	
r(O···O)	2.452(s), 5.895(t)	2.366(s), 4.390(t)	2.363(s), 3.033(t)	2.363(s), 2.958(t)	
r($Cu^+\cdots O_w$)		1.979(s), 2.037(t)	2.097(s), 2.111(t)	2.077(s), 2.100(t)	
a($Cu^+\cdots$NO)	117.7(s), 180.0(t)	123.1(s), 146.0(t)	124.3(s), 133.4(t)	124.7(s), 134.2(t)	
a(N···$Cu^+\cdots$N)	97.2(s), 180.0(t)	91.3(s), 124.5(t)	90.7(s), 99.0(t)	90.6(s), 96.7(t)	
			X = H_2O[e]		
r($Cu^+\cdots O_w$)	1.940	1.919	1.983, 2.196		2.140
r(H−O_w)	0.985	0.984	0.981, 0.982		0.982
a(H−O_w−H)	106.9	106.9	105.9, 106.1		104.7
a($Cu^+\cdots O_w$−H)	119.3	118.4−118.7	115.3−126.9		111.0, 118.6
a($O_w\cdots Cu^+\cdots O_w$)		177.2	99.9, 160.2		99.3, 132.6

[a] Bond lengths in angstroms. Angles in degrees. Models displayed in Figures 1−5. [b] Calculated geometry of the free CO and CO^+ molecules: r(C−O) = 1.150 and 1.137 Å, respectively. [c] Calculated geometry of the free NO and NO^+ molecules: r(N−O = 1.176 and 1.088 Å, respectively. [d] Calculated geometry of the free NO dimer: r(N−O) = 1.176 Å, r(N···N) = 2.089 Å, and r(O···O) = 2.436 Å. (s) and (t) refer to geometry of the singlet and triplet state, respectively. [e] Calculated geometry of the free water molecule: r(H−O_w) = 0.980 Å and a(H−O_w−H) = 102.7°.

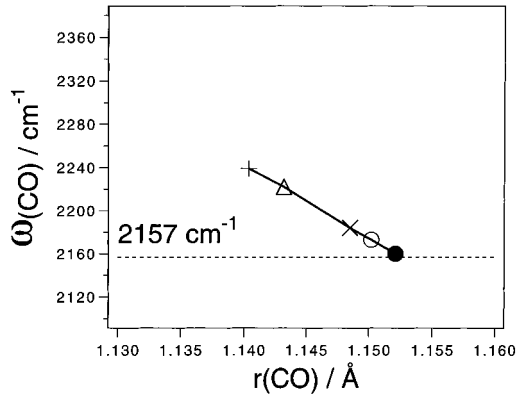

Figure 6. Evolution of stretching frequency ω(CO) and bond length r(CO) in $(H_2O)_n\cdots Cu^+\cdots$CO molecular models with increasing n: n = 0, (+); n = 1, (△); n = 2, (×); n = 2 + 1, (○); n = 3, (●).

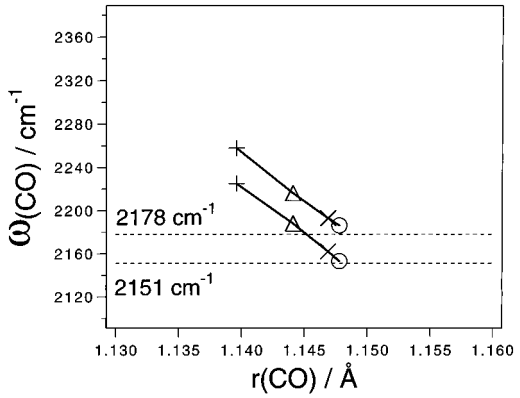

Figure 7. Evolution of stretching frequencies ω(CO) and bond length r(CO) in $(H_2O)_n\cdots Cu^+\cdots 2$(CO) molecular models with increasing n: n = 0, (+); n = 1, (△); n = 2, (×); n = 2 + 1, (○).

so that at $n = 3$ the scaled ω(CO) value differs from experiment by only 3 cm^{-1} (see Figure 6).

When two CO molecules are adsorbed, forming the $(H_2O)_n\cdots Cu^+\cdots 2$(CO) models, the antisymmetric and symmetric ω(CO) values undergo changes similar to those of a single adsorbed CO molecule but the frequency separation between the antisymmetric and symmetric ω(CO) values remains constant at about 30 cm^{-1} for all n values. In comparison with experiment, we note that $(H_2O)_{2+1}\cdots Cu^+\cdots 2$(CO) produces antisymmetric and symmetric scaled ω(CO) values that agree with the experimental 2151 and 2178 cm^{-1} bands in both magnitude and frequency separation (see Figure 7).

Table 4 lists the stretching frequencies ω(NO) of the adsorbed NO molecules in the $(H_2O)_n\cdots Cu^+\cdots$NO and $(H_2O)_n\cdots Cu^+\cdots (NO)_2$ models. Similar to the case of adsorbed CO, the stretching frequencies ω(NO) of the adsorbed NO molecules decrease as the number of water molecules n is increased. However, unlike CO, the ω(NO) value of one adsorbed NO at $n = 0$ is not greater than its free molecule value. Hence, as n water molecules are added and the ω(NO) values decrease, the stretching frequencies ω(NO) of the $(H_2O)_n\cdots Cu^+\cdots$NO models turn out to be red shifted with respect to free NO. Comparing the scaled ω(NO) values of the $(H_2O)_n\cdots Cu^+\cdots$NO models with

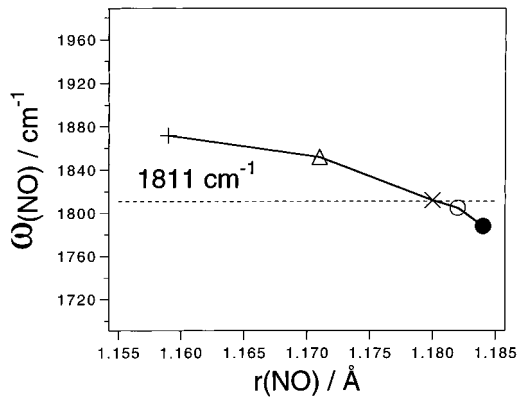

Figure 8. Evolution of stretching frequency ω(NO) and bond length r(NO) in $(H_2O)_n\cdots Cu^+\cdots NO$ molecular models with increasing n: $n = 0$, (+); $n = 1$, (△); $n = 2$, (×); $n = 2 + 1$, (○); $n = 3$, (●).

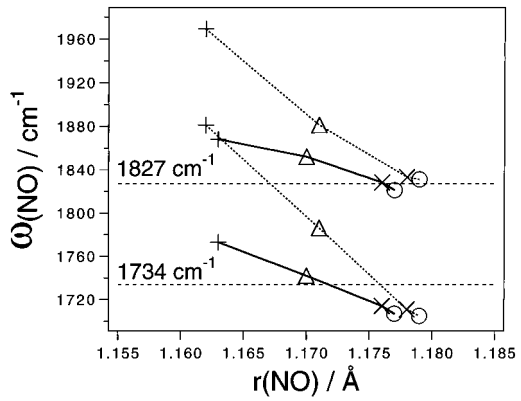

Figure 9. Evolution of stretching frequencies ω(NO) and bond length r(NO) in $(H_2O)_n\cdots Cu^+\cdots(NO)_2$ molecular models with increasing n: Solid line, singlet state; dotted line, triplet state; $n = 0$, (+); $n = 1$, (△); $n = 2$, (×); $n = 2 + 1$, (○).

TABLE 2: Mulliken Charges of Selected Atoms in $(H_2O)_n\cdots Cu^+\cdots X$ Models[a]

charge	$n = 0$	$n = 1$	$n = 2$	$n = 2 + 1$	$n = 3$
			X = CO		
$q(Cu^+)$	0.833	0.703	0.557	0.547	0.395
$q(C) + q(O)$	0.167	0.099	0.034	0.009	0.027
			$X = (CO)_2$		
$q(Cu^+)$	0.695	0.574	0.367	0.329	
$q(C) + q(O)$	0.153	0.114	0.117	0.101	
			X = NO		
$q(Cu^+)$	0.845	0.816	0.676	0.660	0.550
$q(N) + q(O)$	0.155	−0.037	−0.110	−0.139	−0.141
			$X = (NO)_2$ [singlet]		
$q(Cu^+)$	0.715	0.701	0.609	0.596	
$q(N) + q(O)$	0.142	0.051	−0.012	−0.034	
			$X = (NO)_2$ [triplet]		
$q(Cu^+)$	1.126	0.884	0.702	0.663	
$q(N) + q(O)$	−0.063	−0.041	−0.052	−0.063	
			$X = H_2O$		
$q(Cu^+)$	0.740	0.550	0.404		0.214

[a] $q(Cu^+)$, q(C), q(O), and q(N) denote the Mulliken charges of atoms in the $(H_2O)_n\cdots Cu^+\cdots X$ models. Note that q(O) refers to the oxygen atoms of the adsorbed CO and NO molecules.

experiment, we note that the experimental band at 1811 cm^{-1} agrees almost exactly with the scaled ω(NO) value of the $n = 2$ model (see Figure 8).

In the case of two adsorbed NO molecules (Table 4), the frequency separation between the antisymmetric and symmetric NO stretching frequencies varies by 19 cm^{-1} in the singlet state and by 38 cm^{-1} in the triplet state as n is increased from $n = 0$ to $n = 2 + 1$. However, as n is increased from $n = 2$ to $n = 2 + 1$, the frequency separation between the antisymmetric and symmetric NO stretching frequencies remains constant in the singlet state and virtually unchanged in the triplet state. A striking feature of Table 4 is that, for two adsorbed NO molecules, the ω(NO) values of the triplet state approach the ω(NO) values of the singlet state as n increases; for example, at $n = 2$ the triplet and singlet states have antisymmetric ω-(NO) values that agree with each other within 3 cm^{-1}, and symmetric ω(NO) values that agree with each other within 5 cm^{-1}. Comparing the experiment, we note that the experimental 1734 and 1827 cm^{-1} bands agree well with the scaled antisymmetric (1711−1714 cm^{-1}) and symmetric (1828−1833 cm^{-1}) ω(NO) values of the $n = 2$ model whereas the $n = 2 + 1$ model affords less qualitative agreement. Hence, the $(H_2O)_2\cdots Cu^+\cdots(NO)_2$ model produces the best agreement with the experimental bands assigned to the dinitrosyl species adsorbed in Cu^+−ZSM-5 (see Figure 9).

The binding energies of CO in $(H_2O)_2\cdots Cu^+\cdots X$ with X = CO and X = 2(CO) are listed in Table 5. Removal of one CO molecule from the models with X = CO and X = 2(CO) requires the highest energy when there are two ligands present on opposite sides of the Cu^+ cation. Thus the largest binding energy of CO occurs at $n = 1$ in the models with X = CO and at $n = 0$ in the models with X = 2(CO). The binding energy of one CO molecule decreases sharply by a factor of 2 as the number of ligands to the Cu^+ cation increases from 2 to 3 which happens as n is increased from 1 to 2 in the models with X = CO and as n is increased from 0 to 1 in the models with X = 2(CO). As the number of ligands to the Cu^+ cation is increased beyond 2, the binding energies of one CO molecule in the models with X = CO and X = 2(CO) vary by less than 6 kcal/mol. It should be pointed out that for X = 2(CO), the binding energy of the second adsorbed CO molecule is smaller than that of the first adsorbed CO molecule. It should also be noted that the energy required to remove both CO molecules from the $(H_2O)_2\cdots Cu^+\cdots 2(CO)$ models in one step is virtually identical to the energy required to remove the two CO molecules in two individual steps, one CO at a time (see Table 5).

The values listed in parentheses in Table 5 are CO binding energies obtained by keeping $(H_2O)_n\cdots Cu^+$ rigid at the geometry of the corresponding $(H_2O)_n\cdots Cu^+\cdots CO$ or $(H_2O)_n\cdots Cu^+\cdots 2$-(CO) molecular models. It is evident that keeping the $(H_2O)_2\cdots Cu^+$ rigid increases the binding energies by 15−20 kcal/mol when $n \geq 2$ which are the cases for which optimization of $(H_2O)_n\cdots Cu^+$ would allow significant changes in position of the water molecules as can be seen by comparing Figures 1 and 5. The experimental estimate of 31.6 kcal/mol for the binding energy of CO on Cu^+ cations in the ZSM-5 zeolite[24] lies between the binding energy values obtained with fully optimized (24.7−28.3 kcal/mol) and rigid (41.5−44.3 kcal/mol) $(H_2O)_n\cdots Cu^+$ for $n = 2$, $2 + 1$, and 3.

Table 6 lists the binding energies of NO in the $(H_2O)_n\cdots Cu^+\cdots X$ models with X = NO and X = $(NO)_2$. The trend in variations of binding energy in the case of NO is similar to the trend in the case of CO, namely, a large binding energy when there are two ligands on opposite sides on the Cu^+ cation and an overall decrease in binding energy with increasing n. However, the binding energies in the case of NO tend to be 10 kcal/mol lower than in the case of CO. Also the fact that two NO molecules form a dimer in the gas phase causes the energy required to remove $(NO)_2$ from $(H_2O)_n\cdots Cu^+\cdots(NO)_2$ to be approximately equal to the sum of the energies required to remove each NO sequentially plus the dimerization energy. The

TABLE 3: Calculated Stretching Vibrational Frequencies of CO in $(H_2O)_n\cdots Cu^+\cdots X$ Models with X = CO and $(CO)_2$[a,b]

	$\sigma\omega$(CO)		$\sigma\Delta\omega$(CO)	
species	$\sigma = 1$	$\sigma = 1.0206$	$\sigma = 1$	$\sigma = 1.0206$
CO	2106	2149	0	0
CO^+	2163	2208	57	59
	X = CO			
$Cu^+\cdots CO$	2194	2239	88	90
$(H_2O)\cdots Cu^+\cdots CO$	2177	2222	71	73
$(H_2O)_2\cdots Cu^+\cdots CO$	2140	2184	34	35
$(H_2O)_{2+1}\cdots Cu^+\cdots CO$	2129	2173	23	24
$(H_2O)_3\cdots Cu^+\cdots CO$	2116	2160	10	11
$Cu^+\cdots CO$ in Cu^+−ZSM-5 (expt)[c]	2157		14	
	X = $(CO)_2$			
$Cu^+\cdots(CO)_2$	2180, 2212	2225, 2258	74, 106	76, 108
$(H_2O)\cdots Cu^+\cdots(CO)_2$	2144, 2171	2188, 2216	38, 65	39, 66
$(H_2O)_2\cdots Cu^+\cdots(CO)_2$	2118, 2149	2162, 2193	12, 43	13, 44
$(H_2O)_{2+1}\cdots Cu^+\cdots(CO)_2$	2110, 2142	2153, 2186	4, 36	4, 37
$Cu^+\cdots(CO)_2$ in Cu^+−ZSM-5 (expt)[c]	2151, 2178		8, 35	

[a] All frequencies are in cm^{-1}. [b] The scaling factor $\sigma = 1.0206$ was determined by fitting the calculated frequencies of CO and CO^+ to their corresponding experimental gas phase values 2143 and 2214 cm^{-1} (see text). [c] From ref 3.

TABLE 4: Calculated Stretching Vibrational Frequencies of NO in $(H_2O)_n\cdots Cu^+\cdots X$ Models with X = NO and $(NO)_2$[a,b]

	$\sigma\omega$(NO)		$\sigma\Delta\omega$(NO)	
species	$\sigma = 1$	$\sigma = 1.0076$	$\sigma = 1$	$\sigma - 1.0076$
NO	1862	1876	0	0
NO^+	2327	2345	465	469
	X = NO			
$Cu^+\cdots NO$	1858	1872	−4	−4
$(H_2O)\cdots Cu^+\cdots NO$	1838	1852	−24	−24
$(H_2O)_2\cdots Cu^+\cdots NO$	1798	1812	−64	−64
$(H_2O)_{2+1}\cdots Cu^+\cdots NO$	1791	1805	−71	−71
$(H_2O)_3\cdots Cu^+\cdots NO$	1775	1788	−87	−88
$Cu^+\cdots NO$ in Cu^+−ZSM-5 (expt)[c]	1811		−64	
	X = $(NO)_2$			
$Cu^+\cdots(NO_2$ [singlet]	1760, 1854	1773, 1868	−102, −8	−103, −8
$Cu^+\cdots(NO)_2$ [triplet]	1867, 1954	1881, 1969	5, 92	5, 93
$(H_2O)\cdots Cu^+\cdots(NO)_2$ [singlet]	1729, 1838	1742, 1852	−133, −24	−134, −24
$(H_2O)\cdots Cu^+\cdots(NO)_2$ [triplet]	1773, 1867	1786, 1881	−89, 5	−90, 5
$(H_2O)_2\cdots Cu^+\cdots(NO)_2$ [singlet]	1701, 1814	1714, 1828	−161, −48	−162, −48
$(H_2O)_2\cdots Cu^+\cdots(NO)_2$ [triplet]	1698, 1819	1711, 1833	−164, −43	−165, −43
$(H_2O)_{2+1}\cdots Cu^+\cdots(NO)_2$ [singlet]	1694, 1807	1707, 1821	−168, −55	−169, −55
$(H_2O)_{2+1}\cdots Cu^+\cdots(NO)_2$ [triplet]	1692, 1817	1705, 1831	−170, −45	−171, −45
$Cu^+\cdots(NO)_2$ in Cu^+−ZSM-5 (expt)[c]	1734, 1827		−141, −48	

[a] All frequencies are in cm^{-1}. [b] The scaling factor $\sigma = 1.0076$ was determined by fitting the calculated frequencies of NO and NO^+ to their corresponding experimental gas phase valeus 1875 and 2345 cm^{-1} (see text). [c] From ref 3.

TABLE 5: Binding Energies of CO in $(H_2O)_n\cdots Cu^+\cdots X$ Models with X = CO and $(CO)_2$[a,b]

species	ΔE^e	ΔE_{ZPE}	$\Delta E^e + \Delta E_{ZPE}$
	X = CO		
$Cu^+\cdots CO \rightarrow Cu^+ + CO$	48.0	−1.5	46.5
$(H_2O)\cdots Cu^+\cdots CO \rightarrow (H_2O)\cdots Cu^+ + CO$	50.7 (50.8)	−1.8	48.9 (49.0)
$(H_2O)_2\cdots Cu^+\cdots CO \rightarrow (H_2O)_2\cdots Cu^+ + CO$	25.9 (45.5)	−1.2	24.7 (44.3)
$(H_2O)_{2+1}\cdots Cu^+\cdots CO \rightarrow (H_2O)_{2+1}\cdots Cu^+ + CO$	31.4 (45.4)	−3.1	28.3 (42.3)
$(H_2O)_3\cdots Cu^+\cdots CO \rightarrow (H_2O)_3\cdots Cu^+ + CO$	29.5 (44.2)	−2.7	26.8 (41.5)
CO on Cu^+−ZSM-5 (IR expt)[c]			31.6
	X = $(CO)_2$		
$Cu^+\cdots(CO)_2 \rightarrow Cu^+\cdots CO + CO$	45.5	−1.7	43.8
$(H_2O)\cdots Cu^+\cdots(CO)_2 \rightarrow (H_2O)\cdots Cu^+\cdots CO + CO$	21.3	−1.1	20.2
$(H_2O)_2\cdots Cu^+\cdots(CO)_2 \rightarrow (H_2O)_2\cdots Cu^+\cdots CO + CO$	16.9	−1.1	15.8
$(H_2O)_{2+1}\cdots Cu^+\cdots(CO)_2 \rightarrow (H_2O)_{2+1}\cdots Cu^+\cdots CO + CO$	14.7	−1.2	13.5
$Cu^+\cdots(CO)_2 \rightarrow Cu^+ + 2CO$	93.5	−3.2	90.3
$(H_2O)\cdots Cu^+\cdots(CO)_2 \rightarrow (H_2O)\cdots Cu^+ + 2CO$	72.0 (73.3)	−2.9	69.1 (70.4)
$(H_2O)_2\cdots Cu^+\cdots(CO)_2 \rightarrow (H_2O)_2\cdots Cu^+ + 2CO$	42.8 (63.6)	−2.3	40.5 (61.3)
$(H_2O)_{2+1}\cdots Cu^+\cdots(CO)_2 \rightarrow (H_2O)_{2+1}\cdots Cu^+ + 2CO$	46.1 (61.1)	−4.3	41.8 (56.8)

[a] All energies in kcal/mol. [b] Values listed in parentheses were obtained by keeping the geometry of $(H_2O)_n\cdots Cu^+$ frozen at that of the corresponding $(H_2O)_n\cdots Cu^+\cdots CO$ or $(H_2O)_n\cdots Cu^+\cdots 2(CO)$ complex. [c] Reference 24.

small differences in binding energies of X = $(NO)_2$ between singlet and triplet electronic states can be traced to the slightly deeper energies of the singlet states for $n \geq 1$.

Table 7 lists the binding energies of H_2O in the $(H_2O)_n\cdots Cu^+\cdots X$ models grouped according to the number of ligands to the Cu^+ cation. It is evident that the binding energies of

TABLE 6: Binding Energies of NO in $(H_2O)_n\cdots Cu^+\cdots X$ Models with X = NO and $(NO)_2$[a,b]

species	ΔE^e	ΔE_{ZPE}	$\Delta E^e + \Delta E_{ZPE}$
X = NO			
$Cu^+\cdots NO \rightarrow Cu^+ + NO$	40.6	−0.9	39.7
$(H_2O)\cdots Cu^+\cdots NO \rightarrow (H_2O)\cdots Cu^+ + NO$	40.8 (40.9)	−1.3	39.5 (39.6)
$(H_2O)_2\cdots Cu^+\cdots NO \rightarrow (H_2O)_2\cdots Cu^+ + NO$	17.9 (36.6)	−0.9	17.0 (35.7)
$(H_2O)_{2+1}\cdots Cu^+\cdots NO \rightarrow (H_2O)_{2+1}\cdots Cu^+ + NO$	23.6 (36.6)	−2.9	20.7 (33.7)
$(H_2O)_3\cdots Cu^+\cdots NO \rightarrow (H_2O)_3\cdots Cu^+ + NO$	20.3 (34.3)	−1.9	18.4 (32.4)
X = $(NO)_2$			
$(NO)_2$ [singlet] → NO + NO	9.7	−1.9	7.8
$Cu^+\cdots(NO)_2$ [singlet] → $Cu^+\cdots NO$ + NO	34.2	−1.9	32.3
$Cu^+\cdots(NO)_2$ [triplet] → $Cu^+\cdots NO$ + NO	41.8	−2.0	39.8
$(H_2O)\cdots Cu^+\cdots(NO)_2$ [singlet] → $(H_2O)\cdots Cu^+\cdots NO$ + NO	23.8	−1.5	22.3
$(H_2O)\cdots Cu^+(NO)_2$ [triplet] → $(H_2O)\cdots Cu^+\cdots NO$ + NO	20.7	−0.8	19.9
$(H_2O)_2\cdots Cu^+\cdots(NO)_2$ [singlet] → $(H_2O)_2\cdots Cu^+\cdots NO$ + NO	21.1	−1.7	19.4
$(H_2O)_2\cdots Cu^+\cdots(NO)_2$ [triplet] → $(H_2O)_2\cdots Cu^+\cdots NO$ + NO	14.3	−0.6	13.7
$(H_2O)_{2+1}\cdots Cu^+\cdots(NO)_2$ [singlet] → $(H_2O)_{2+1}\cdots Cu^+\cdots NO$ + NO	20.0	−1.6	18.4
$(H_2O)_{2+1}\cdots Cu^+\cdots(NO)_2$ [triplet] → $(H_2O)_{2+1}\cdots Cu^+\cdots NO$ + NO	16.0	−0.9	15.1
$Cu^+\cdots(NO)_2$ [singlet] → $Cu^+ + (NO)_2$	65.2	−0.8	64.4
$Cu^+\cdots(NO)_2$ [triplet] → $Cu^+ + (NO)_2$	72.8	−1.0	71.8
$(H_2O)\cdots Cu^+\cdots(NO)_2$ [singlet] → $(H_2O)\cdots Cu^+ + (NO)_2$	55.0 (55.5)	−0.8	54.2 (54.7)
$(H_2O)\cdots Cu^+\cdots(NO)_2$ [singlet] → $(H_2O)\cdots Cu^+ + (NO)_2$	51.8 (53.0)	−0.1	51.7 (52.9)
$(H_2O)_2\cdots Cu^+\cdots(NO)_2$ [singlet] → $(H_2O)_2\cdots Cu^+ + (NO)_2$	29.4 (49.1)	−0.6	28.8 (48.5)
$(H_2O)_2\cdots Cu^+\cdots(NO)_2$ [triplet] $(H_2O)_2\cdots Cu^+ + (NO)_2$	24.3 (44.2)	0.2	24.5 (44.4)
$(H_2O)_{2+1}\cdots Cu^+\cdots(NO)_2$ [singlet] → $(H_2O)_{2+1}\cdots Cu^+ + (NO)_2$	34.0 (47.9)	−2.5	31.5 (45.4)
$(H_2O)_{2+1}\cdots Cu^+\cdots(NO)_2$ [triplet] → $(H_2O)_{2+1}\cdots Cu^+ + (NO)_2$	28.3 (42.6)	−1.6	26.7 (41.0)

[a] All energies in kcal/mol. [b] Values listed in parentheses were obtained by keeping the geometry of $(H_2O)_n\cdots Cu^+$ frozen at that of the corresponding $(H_2O)_n\cdots Cu^+\cdots NO$ or $(H_2O)_n\cdots Cu^+\cdots(NO)_2$ complex.

TABLE 7: Binding Energies of H_2O in $(H_2O)_n\cdots Cu^+\cdots X$ Models with X = CO, 2(CO), NO, 2(NO), and H_2O[a]

species	ΔE^e	ΔE_{ZPE}	$\Delta E^e + \Delta E_{ZPE}$
4 ligands on Cu^+			
$(H_2O)_2\cdots 2(CO) \rightarrow (H_2O)\cdots Cu^+\cdots 2(CO) + H_2O$	22.8	−2.1	20.7
$(H_2O)\cdots Cu^+\cdots(NO)_2$ [singlet] → $(H_2O)\cdots Cu^+\cdots(NO)_2$ [singlet] + H_2O	26.4	−2.5	23.9
$(H_2O)_2\cdots Cu^+\cdots(NO)_2$ [triplet] → $(H_2O)\cdots Cu^+\cdots(NO_2)$ [triplet] + H_2O	24.4	−2.3	22.1
$(H_2O_3\cdots Cu^+\cdots CO \rightarrow (H_2O)_2\cdots Cu^+\cdots CO + H_2O$	22.8	−2.7	20.1
$(H_2O)_3\cdots Cu^+\cdots NO \rightarrow (H_2O)_2\cdots NO \rightarrow Cu^+\cdots NO + H_2O$	21.5	−2.2	19.3
$(H_2O)_4\cdots Cu^+ \rightarrow (H_2O)_3\cdots Cu^+ + H_2O$	16.2	−1.9	14.3 (15 ± 2)[b]
3 ligands on Cu^+			
$(H_2O)_2\cdots Cu^+\cdots CO \rightarrow (H_2O)\cdots Cu^+\cdots CO + H_2O$	27.2	−2.1	25.1
$(H_2O)_2\cdots Cu^+\cdots NO \rightarrow (H_2O)\cdots Cu^+\cdots NO + H_2O$	29.1	−2.3	26.8
$(H_2O)\cdots Cu^+\cdots 2(CO) \rightarrow Cu^+\cdots 2(CO) + H_2O$	31.1	−1.7	29.4
$(H_2O)\cdots Cu^+\cdots(NO)_2$ [singlet] → $Cu^+\cdots(NO)_2$ [singlet] + H_2O	42.3	−1.9	40.4
$(H_2O)\cdots Cu^+\cdots(NO)_2$ [triplet] → $Cu^+\cdots(NO)_2$ [triplet] + H_2O	31.6	−1.1	30.5
$(H_2O)_3\cdots Cu^+ \rightarrow (H_2O)_2\cdots Cu^+ + H_2O$	19.2	−1.2	18.0 (17 ± 2)[b]
2 ligands on Cu^+			
$(H_2O)\cdots Cu^+\cdots CO \rightarrow Cu^+\cdots CO + H_2O$	55.2	−2.3	52.9
$(H_2O)\cdots Cu^+\cdots NO \rightarrow Cu^+\cdots NO + H_2O$	52.7	−2.3	50.4
$(H_2O)_2\cdots Cu^+ \rightarrow (H_2O)\cdots Cu^+ + H_2O$	52.0	−2.7	49.3 (39 ± 3)[b]
1 ligand on Cu^+			
$(H_2O)\cdots Cu^+ \rightarrow Cu^+ + H_2O$	52.5	−2.0	50.5 (35 ± 3)[b]
hydrogen-bonded water			
$(H_2O)_{2+1}\cdots Cu^+\cdots CO \rightarrow (H_2O)_2\cdots Cu^+\cdots CO + H_2O$	24.7	−3.1	21.6
$(H_2O)_{2+1}\cdots Cu^+\cdots 2(CO) \rightarrow (H_2O)_2\cdots Cu^+\cdots 2(CO) + H_2O$	22.5	−3.2	19.3
$(H_2O)_{2+1}\cdots Cu^+\cdots NO \rightarrow (H_2O)_2\cdots Cu^+\cdots NO + H_2O$	24.9	−3.2	21.7
$(H_2O)_{2+1}\cdots Cu^+\cdots(NO)_2$ [singlet] → $(H_2O)_2\cdots Cu^+\cdots(NO)_2$ [singlet] + H_2O	23.8	−3.1	20.7
$(H_2O)_{2+1}\cdots Cu^+\cdots(NO)_2$ [triplet] → $(H_2O)_2\cdots Cu^+\cdots(NO)_2$ [triplet] + H_2O	23.2	−2.9	20.3

[a] All energies in kcal/mol. [b] Experimental values are listed in parentheses (ref 26).

H_2O tend to increase as the number of ligands to the Cu^+ cation decreases. Consistent with previous theoretical work[25] on the successive binding energies of H_2O in $(H_2O)_n\cdots Cu^+$, agreement between our calculated values and those of experiment[26] improves with increasing n; this indicates that binding energies calculated for our $(H_2O)_n\cdots Cu^+\cdots X$ complexes containing three or more ligands are in fact quite accurate, within the limitations of the molecular models. S_4 symmetry was imposed in the $n = 4$ case to avoid unrealistically large hydrogen bonding among the water molecules.[27] For the sake of completeness, Table 7 also includes the binding energy of the hydrogen-bonded water molecule in the $n = 2 + 1$ arrangement. It is clear that the binding energy and zero-point energy contribution of the hydrogen-bonded water molecule hardly discriminate among the various adsorbed molecules X = CO, 2(CO), NO, and $(NO)_2$.

IV. Discussion

As noted in the previous section, Tables 1−4 indicate that the bond length, Mulliken charge, and frequency of the X molecules adsorbed on the Cu^+ cation, with X = CO, 2(CO), NO, or $(NO)_2$, are sensitive to the number of water molecules

in the molecular model. Thus the adsorbed X molecules undergo the following changes: their bond lengths increase, their Mulliken charges become more negative, and their stretching frequencies decrease as the number n of water molecules is increased. This is consistent with the assumption that the amount of charge transferred to the adsorbed X molecules from the water molecules through the Cu^+ cation is intimately related to the bond lengths and stretching frequencies of the adsorbed X molecules. Therefore, we can speculate that as the X molecules adsorb on the Cu^+ cation in the $Cu^+-ZSM-5$ zeolite, their stretching frequencies are also dependent on the amount of charge transferred to them from the zeolite framework through the Cu^+ cation.

This charge transfer is consistent with the usual description[28] of bonding between CO and metal surfaces in terms of charge donation from the antibonding 5σ orbital of CO into the vacant metal orbitals and back-donation from the occupied metal d orbitals into the vacant antibonding 2π orbitals of CO. The CO^+ character of the adsorbed CO molecule in the $Cu^+\cdots CO$ model (made evident by the 90 cm^{-1} increase in the ω(CO) stretching frequency, the decrease in r(C-O) bond length, and the net positive Mulliken charge) suggests that charge donation from CO to Cu^+ dominates over back-donation from Cu^+ to CO; however, as n is increased from 0 to 3, back-donation appears to become more important and the ω(CO) stretching frequencies decrease. It is noteworthy, however, that, in agreement with experimental IR studies of CO in $Cu^+-ZSM-5$ zeolite,[3] the ω(CO) stretching frequencies of the $(H_2O)_n\cdots Cu^+\cdots CO$ models are blue shifted with respect to free CO.

The fact that, in spite of the decrease in r(NO) bond length, the stretching frequency ω(NO) in the $Cu^+\cdots NO$ complex remains equal to that of the free NO molecule (see Tables 1 and 4) suggests that the charge transfer mechanism from the NO molecule to the Cu^+ cation is different from that of the CO molecule. The molecular orbitals of the $Cu^+\cdots NO$ complex reveal that the unpaired π electron of the NO molecule is partly donated to the unoccupied 4s orbital of the Cu^+ cation thus competing against the charge transfer from the 5σ orbital of NO to the same 4s orbital in the Cu^+ cation. Since such competition is not present in the $Cu^+\cdots CO$ complex, we attribute both the virtually unchanged ω(NO) frequency and bent $Cu^+\cdots NO$ angle to the interaction between the unpaired electron of NO and the formerly empty 4s orbital of Cu^+. Then, as water molecules are added, forming the $(H_2O)_n\cdots Cu^+\cdots NO$ models, charge is transferred to the adsorbed NO, decreasing its ω(NO) frequency so that it is red shifted with respect to free NO in agreement with experimental IR studies of NO in $Cu^+-ZSM-5$ zeolite.[3]

Comparing the calculated stretching frequencies ω(CO) and those from experiment (see Table 3), we noted that the scaled ω(CO) value of the $(H_2O)_3\cdots Cu^+\cdots CO$ molecular model agrees with the 2157 cm^{-1} band. The scaled ω(CO) values of the antisymmetric and symmetric stretching frequencies of the $(H_2O)_{2+1}\cdots Cu^+\cdots 2(CO)$ model also agree with the measured 2151 and 2178 cm^{-1} bands, respectively. It is interesting that in both of these models there are four ligands to the Cu^+ cation; therefore, comparison between the scaled ω(CO) values of our molecular models and the experimental IR bands suggests that a water ligand is lost when a second CO molecule is adsorbed on the Cu^+ cation so that the number of ligands to the Cu^+ cation can reach a maximum of four. A similar idea was recently proposed by Lamberti et al.[3b] who, on the basis of a spectroscopic study of $Cu^+-ZSM-5$, inferred that there are two types of Cu^+ cations. According to these authors, one type of Cu^+ cations is surrounded by three nearest neighbor framework oxygens and is able to adsorb up to two CO molecules whereas the other type of Cu^+ cations is surrounded by two nearest neighbor framework oxygens and is able to adsorb up to three CO molecules so that the number of ligands to both types of the Cu^+ cations in $Cu^+-ZSM-5$ under CO pressure can reach a maximum of five ligands at 110−120 K.

The trend of a constant number of ligands upon adsorption of a second CO molecule found in our the molecular models is not as conspicuous in the case of NO adsorption. However, our NO adsorption results still indicate that (a) less charge is transferred to the adsorbed molecules when $X = (NO)_2$ than when $X = NO$ (see Table 2), and (b) there is good agreement between the experimental 1734 and 1827 cm^{-1} bands (assigned to the dinitrosyl species adsorbed in the $Cu^+-ZSM-5$ zeolite) and the antisymmetric and symmetric scaled ω(NO) values of the $(H_2O)_2\cdots Cu^+\cdots(NO)_2$ model and between the experimental 1811 cm^{-1} band (assigned to the mononitrosyl species adsorbed in the $Cu^+-ZSM-5$ zeolite) and the scaled ω(NO) values of both the $(H_2O)_2\cdots Cu^+\cdots NO$ and $(H_2O)_{2+1}\cdots Cu^+\cdots NO$ models (see Table 4). Hence, agreement between the scaled stretching frequencies ω(NO) of $(H_2O)_n\cdots Cu^+\cdots NO$ and $(H_2O)_n\cdots Cu^+\cdots(NO)_2$ models and the experimental IR spectra still shows a subtle preference for a decrease in the number of water molecules when a second NO molecule is adsorbed.

With regard to the adsorption of two molecules $X = 2(CO)$ and $X = (NO)_2$ in the $(H_2O)_2\cdots Cu^+\cdots X$ models, we note a correlation between the angle formed by the adsorbed molecules and the frequency separation between the antisymmetric and symmetric stretching frequencies of the adsorbed molecules. Thus $(H_2O)_2\cdots Cu^+\cdots 2(CO)$ has a relatively wide $C\cdots Cu^+\cdots C$ angle of 122.1° and a relatively narrow frequency separation of 31 cm^{-1} between the antisymmetric and symmetric CO stretching frequencies, whereas $(H_2O)_2\cdots Cu^+\cdots(NO)_2$ has relatively narrow $N\cdots Cu^+\cdots N$ angles of 90.7° (singlet) and 99.0° (triplet) and relatively wide frequency separations of 113 cm^{-1} (singlet) and 121 cm^{-1} (triplet) between the antisymmetric and symmetric NO stretches. It should also be pointed out that since the scaled ω(NO) values of the singlet and triplet states of $(H_2O)_2\cdots Cu^+\cdots(NO)_2$ are both close to the experimental bands assigned to the dinitrosyl species adsorbed in the $Cu^+-ZSM-5$ zeolite, it seems possible that both the singlet and the triplet states of the adsorbed dinitrosyl may be present in the IR spectra with the singlet state being the dominant species since $(H_2O)_2\cdots Cu^+\cdots(NO)_2$ is 5.1 kcal/mol more stable in the singlet state than in the triplet state.

We now investigate the competition between a water and a CO molecule for formation of a fourth ligand to the Cu^+ cation in the $(H_2O)_2\cdots Cu^+\cdots CO$ model. Insight into the adsorption energetics can be obtained by considering the reaction

$$(H_2O)_2\cdots Cu^+\cdots 2(CO) + H_2O \rightarrow (H_2O)_3\cdots Cu^+\cdots CO + CO$$

which is energetically favored by 6.2 kcal/mol. Therefore, the Cu^+ cation in the $(H_2O)_2\cdots Cu^+\cdots CO$ model prefers to form its fourth ligand with a water molecule than with a CO molecule. This is because the binding energy of the second CO molecule is about half the binding energy of the first CO and is also less than the binding energy of an additional water molecule. Hence, the molecular models suggest that formation of the dicarbonyl species adsorbed on the Cu^+ cation may be slightly hindered energetically. This is consistent with the fact that the appearance of the IR spectral bands that correspond to the dicarbonyl species in $Cu^+-ZSM-5$ requires relatively high CO pressures and/or low temperatures.[3]

In the case of NO adsorption, the second adsorbed NO molecule has a binding energy comparable to that of the first one. For example, the binding energy of the second NO molecule to the $(H_2O)_2\cdots Cu^+\cdots NO$ model, forming a singlet state, is comparable to that of the first NO (see Table 6) and to that of a third water molecule (see Table 7). Consequently, in the reaction

$$(H_2O)_2\cdots Cu^+\cdots (NO)_2[\text{singlet}] + H_2O \rightarrow (H_2O)_3\cdots Cu^+\cdots NO + NO$$

the energy of the left-hand side is equal to that of the right-hand side (within 0.2 kcal/mol). Therefore, energetically the fourth ligand to the Cu^+ cation in the $(H_2O)_2\cdots Cu^+\cdots NO$ model can be formed with either a water molecule or a second NO. Hence, the molecular models suggest that the formation of the adsorbed dinitrosyl species adsorbed on the Cu^+ cation is energetically allowed. This result is consistent with the fact that the IR spectral bands that correspond to the dinitrosyl species are readily observed at room temperature.[3]

As mentioned in the Results section, the binding energies of CO and NO in the $(H_2O)_n\cdots Cu^+\cdots X$ molecular models increase by up to 20 kcal/mol for $n \geq 2$ when the $(H_2O)_n\cdots Cu^+$ models are kept rigid at the geometry of the corresponding $(H_2O)_n\cdots Cu^+\cdots X$ (see Table 5 and 6). We calculated the binding energies in both the rigid and optimized $(H_2O)_n\cdots Cu^+$ approximations because we suspected that the oxygen atoms of the zeolite framework may not be as floppy as the ones in our molecular models. Even though our goal was not to calculate accurate binding energies on an absolute scale, it is nevertheless gratifying that the experimental estimate of 31.6 kcal/mol for the binding energy of CO to the Cu^+ cation in $Cu^+-ZSM\text{-}5$[24] does in fact lie between the binding energy values obtained with the rigid and optimized $(H_2O)_n\cdots Cu^+$ approximations for $n \geq 2$. It should also be pointed out that, according to Table 7, the successive binding energies of water in the $(H_2O)_n\cdots Cu^+$ models agree with experiment[26] within 1 kcal/mol when there are three or more ligands to the Cu^+ cation.

V. Conclusions

We have attempted to analyze the experimental IR spectra of CO and NO adsorbed in $Cu^+-ZSM\text{-}5$ zeolite samples by means of quantum mechanical density functional calculations employing molecular models of the form $(H_2O)_n\cdots Cu^+\cdots X$ in which charge transfer from the oxygen atoms of the zeolite framework to the Cu^+ cation and the adsorbed X molecules is represented by water molecules coordinated to the Cu^+ cation. Good agreement with experiment is established. The following conclusions can be derived from the present work:

(1) The stretching frequency shifts experienced by CO and NO upon adsorption in $Cu^+-ZSM\text{-}5$ are partly due to (i) transfer of negative charge from electron-donating oxygen atoms to the adsorbed molecules through the Cu^+ cation and (ii) the absence (in CO) or presence (in NO) of an antibonding unpaired electron in the adsorbed molecule. When the CO molecule adsorbs on a Cu^+ cation, forming the $Cu^+\cdots CO$ complex, the $Cu^+\cdots CO$ bond is linear, the CO molecule donates charge to the Cu^+ cation, and the CO molecule undergoes a relatively large blue shift in its ω(CO) stretching frequency relative to the gas phase value. As electron-donating oxygen atoms form ligands to the Cu^+ cation, charge is transferred back to the adsorbed CO molecule thus decreasing its ω(CO) stretching frequency so that the net effect is a relatively small blue shift. On the other hand, when the NO molecule adsorbs on a Cu^+ cation, it forms a bent $Cu^+\cdots NO$ bond and its ω(NO) stretching frequency remains almost unchanged from the gas phase value due to interaction between the antibonding unpaired electron present in the NO molecule and the Cu^+ cation. Nevertheless, similar to the case of CO, as oxygen atoms form ligands to the Cu^+ cation, charge is back-transferred to the adsorbed NO, thus decreasing its ω(NO) stretching frequency so that the net effect in ω(NO) is a relatively large red shift.

(2) The absence or presence of an antibonding unpaired electron in the adsorbed molecule(s) also affects the formation of dicarbonyl and dinitrosyl species in $Cu^+-ZSM\text{-}5$ and the separation in frequency between their antisymmetric and symmetric stretching modes. Formation of the dicarbonyl species is hindered by the mutual repulsion between the two adsorbed CO molecules and by competition for ligand formation between the Cu^+ cation and an oxygen atom. On the other hand, formation of the adsorbed dinitrosyl species in the singlet state is favored by the mutual attraction among the two adsorbed NO molecules due to the partial pairing of the formerly unpaired electron in each NO molecule. Thus in the dicarbonyl species the second adsorbed CO is less strongly bound than the first CO, whereas in the adsorbed dinitrosyl species the second NO is as or more strongly bound as/than the first NO. The dicarbonyl species also has, as a consequence of repulsion between the two adsorbed CO molecules, a relatively wide $C\cdots Cu^+\cdots C$ angle (121°); whereas the dinitrosyl species, due to the attraction between the two adsorbed NO molecules, affords a narrower $N\cdots Cu^+\cdots N$ angle (91−99°). The separation in frequency between the antisymmetric and symmetric stretching modes is sensitive to this geometrical difference. To the dicarbonyl species, having a wide $C\cdots Cu^+\cdots C$ angle, corresponds a narrow frequency separation of 31 cm^{-1} between its antisymmetric and symmetric stretching modes. To the dinitrosyl species, which has a narrow $N\cdots Cu^+\cdots N$ angle, corresponds a wide frequency separation of 113−121 cm^{-1} between its antisymmetric and symmetric stretching modes.

(3) Comparison between the measured bands in the IR spectra of CO adsorbed in $Cu^+-ZSM\text{-}5$ and the scaled stretching frequencies ω(CO) of the $(H_2O)_n\cdots Cu^+\cdots CO$ and $(H_2O)_n\cdots Cu^+\cdots 2(CO)$ models suggests that the number of ligands to the Cu^+ cation remains constant as the number of adsorbed CO molecules increases from 1 to 2. Hence, the number of oxygen ligands to the Cu^+ cation decreases from 3 to 2 as the number of adsorbed CO molecules increases from 1 to 2. This trend of a constant number of ligands to the Cu^+ cation upon adsorption of a second CO molecule is not as sharply evident in the case of NO adsorption, but agreement between the scaled stretching frequencies ω(NO) of $(H_2O)_n\cdots Cu^+\cdots NO$ and $(H_2O)_n\cdots Cu^+\cdots (NO)_2$ models and the experimental IR spectra still shows a subtle preference for a decrease in the number of water molecules from the models when a second NO molecule is adsorbed.

(4) The experimental estimate of 31.6 kcal/mol for the binding energy of CO to the Cu^+ cation in $Cu^+-ZSM\text{-}5$ does in fact lie between the binding energy values obtained with the rigid and optimized $(H_2O)_n\cdots Cu^+$ approximations for $n \geq 2$. In addition, the calculated successive binding energies of water in $(H_2O)_n\cdots Cu^+$ agree with the experimental values within 1 kcal/mol when there are three or more ligands to the Cu^+ cation.

Acknowledgment. This work was partly carried out under the auspices of the U.S. Department of Energy, Office of Industrial Technologies. We gratefully acknowledge conversations with Drs. Richard L. Martin, Janos Szanyi, and Mark T. Paffett.

References and Notes

(1) Shelef, M. *Chem. Rev.* **1995**, *95*, 209.

(2) Iwamoto, M.; Yokoo, S.; Sakai, K.; Kagawa, S. *J. Chem. Soc., Faraday Trans. 1* **1981**, *77*, 1629.

(3) (a) Spoto, G.; Zecchina, A.; Bordiga, S.; Ricchiardi, G.; Martra, G. *Appl. Catal. B* **1994**, *3*, 151. (b) Lamberti, C.; Bordiga, S.; Salvalaggio, M.; Spoto, G.; Zecchina, A.; Geobaldo, F.; Vlaic, G.; Bellatreccia, M. *J. Phys. Chem. B* **1997**, *101*, 344.

(4) Marquez-Alvares, C.; McDougall, G. S.; Guerrero-Ruiz, A.; Rodriguez-Ramos, I. *Appl. Surf. Sci.* **1994**, *78*, 477.

(5) Giamello, E.; Murphy, D.; Magnacca, G.; Morterra, C.; Shioya, Y.; Nomura, T.; Anpo, M. *J. Catal.* **1992**, *136*, 510.

(6) Spoto, G.; Bordiga, S.; Scarano, D.; Zecchina, A. *Catal. Lett.* **1992**, *13*, 39.

(7) (a) Anpo, M.; Matsuoka, M.; Shioya, Y.; Yamashita, H.; Giamello, E.; Morterra, C.; Che, M.; Patterson, H. H.; Webber, S.; Oullette, S.; Fox, M. A. *J. Phys. Chem.* **1994**, *98*, 5744. (b) Yamashita, H.; Matsuoka, M.; Tsuji, K.; Shioya, Y.; Anpo, M.; Che, M. *J. Phys. Chem.* **1996**, *100*, 397.

(8) Valyon, J.; Hall, W. K. *J. Phys. Chem.* **1993**, *97*, 1204.

(9) Itho, Y.; Nishiyama, S.; Tsuruya, S.; Masai, M. *J. Phys. Chem.* **1994**, *98*, 960.

(10) Sass, C. E.; Kevan, L. *J. Phys. Chem.* **1988**, *92*, 5192 and references therein.

(11) (a) Sauer, J. *Chem. Rev.* **1989**, *89*, 199. (b) Sauer, J.; Ugliengo, P.; Garrone, E.; Saunders, V. R. *Chem. Rev.* **1994**, *94*, 2095.

(12) (a) Trout, B. L.; Chakraborty, A. K.; Bell, A. T. *J. Phys. Chem.* **1996**, *100*, 4173−4179. (b) Yokomichi, Y.; Yamabe, T.; Ohtsuka, H.; Kakumoto, T. *J. Phys. Chem.* **1996**, *100*, 14424. (c) Blint, R. J. *J. Phys. Chem.* **1996**, *100*, 19518. (d) Zhanpeisov, N. U.; Nakatsuji, H.; Hada, M.; Nakai, H.; Anpo, M. *Catal. Lett.* **1996**, *42*, 173.

(13) (a) Hass, K. C.; Schneider, W. F. *J. Phys. Chem.* **1996**, *100*, 9292−9301. (b) Ramprasad, R.; Schneider, W. F.; Hass, K. C.; Adams, J. B. *J. Phys. Chem. B* **1997**, *101*, 1940.

(14) Huber, K. P.; Herzberg, G. *Constants of Diatomic Molecules*; Van Nostrand Reinhold: New York, 1979.

(15) Laane, J.; Ohlsen, J. R. *Prog. Inorg. Chem.* **1980**, *27*, 465.

(16) Rauhut, G.; Pulay, P. *J. Phys. Chem.* **1995**, *99*, 3093.

(17) Johnson, B. G.; Gill, P. M. W.; Pople, J. A. *J. Chem. Phys.* **1993**, *98*, 5612.

(18) Becke, A. D. *Phys. Rev. A* **1988**, *38*, 3098.

(19) Lee, C.; Yang, W.; Parr, R. G. *Phys. Rev. B* **1988**, *37*, 785.

(20) Hehre, W. J.; Radom, L.; Schleyer, P. v. R.; Pople, J. A. *Ab Initio Molecular Orbital Theory*; Wiley-Interscience: New York, 1986; p 82 and references therein.

(21) Wachters, A. J. H. *J. Chem. Phys.* **1970**, *52*, 1033.

(22) Hay, P. J. *J. Chem. Phys.* **1977**, *66*, 4377.

(23) Frisch, M. J.; Trucks, G. W.; Schlege, H. B.; Gill, P. M. W.; Johnson, B. G.; Robb, M. A.; Cheeseman, J R.; Keith, T.; Petersson, G. A.; Montgomery, J. A.; Raghavachari, K.; Al-Laham, M. A.; Zakrzewski, V. G.; Ortiz, J. V.; Foresman, J. B.; Cioslowski, J.; Stefanov, B. B.; Nanayakkara, A.; Challacombe, M.; Peng, C. Y.; Ayala, P. Y.; Chen, W.; Wong, M. W.; Andres, J. L.; Replogle, E. S.; Gomperts, R.; Martin, R. L.; Fox, D. J.; Binkley, J. S.; Defrees, D. J.; Baker, J.; Stewart, J. P.; Head-Gordon, M.; Gonzalez, C.; Pople, J. A. *Gaussian 94, Revision D.3*; Gaussian, Inc.: Pittsburgh, PA, 1995.

(24) Szanyi, J.; Paffett, M. T. Unpublished results, 1995.

(25) Bauschlicher, C. W.; Langhoff, S. R.; Partridge, H. *J. Chem. Phys.* **1991**, *94*, 2068.

(26) Magnera, T. F.; David, D. E.; Stulik, D.; Orth, R. G.; Jonkman, H. T.; Michl, J. *J. Am. Chem. Soc.* **1989**, *111*, 5036.

(27) Del Bene, J. E.; Person, W. B.; Szczepaniak, K. *J. Phys. Chem.* **1995**, *99*, 10705.

(28) (a) Campbell, I. M. *Catalysis at Surfaces*; Chapman and Hall: New York, 1988; p 139. (b) Salomon, E. I.; Jones, P. M.; May, J. A. *Chem. Rev.* **1993**, *93*, 2623.